Received: 29 October 2022 | Revised: 26 January 2023 | Accepted: 15 February 2023

DOI: 10.1002/jbm.a.37520

RESEARCH ARTICLE

Elastin-like protein hydrogels with controllable stress relaxation rate and stiffness modulate endothelial cell function

Mahdis Shayan[1,2] | Michelle S. Huang[3] | Renato Navarro[4] | Gladys Chiang[5] | Caroline Hu[5] | Beu P. Oropeza[1,2,5] | Patrik K. Johansson[6] | Riley A. Suhar[4] | Abbygail A. Foster[4] | Bauer L. LeSavage[7] | Maedeh Zamani[1,2] | Annika Enejder[6] | Julien G. Roth[8] | Sarah C. Heilshorn[2,3,4,6] | Ngan F. Huang[1,2,3,5]

[1]Department of Cardiothoracic Surgery, Stanford University, Palo Alto, California, USA

[2]The Stanford Cardiovascular Institute, Stanford University, Palo Alto, California, USA

[3]Department of Chemical Engineering, Stanford University, Palo Alto, California, USA

[4]Department of Materials Science & Engineering, Stanford University, Palo Alto, California, USA

[5]Center for Tissue Regeneration, Repair and Restoration, Veterans Affairs Palo Alto Health Care System, Palo Alto, California, USA

[6]Geballe Laboratory for Advanced Materials, Stanford University, Palo Alto, California, USA

[7]Department of Bioengineering, Stanford University, Palo Alto, California, USA

[8]Institute for Stem Cell Biology & Regenerative Medicine, Stanford University School of Medicine, Palo Alto, California, USA

Correspondence
Ngan F. Huang, Department of Cardiothoracic Surgery, Stanford University, 300 Pasteur Drive, MC 5407, Stanford, CA 94305-5407, USA.
Email: ngantina@stanford.edu

Sarah C. Heilshorn, Department of Materials Science & Engineering, Stanford University, 476 Lomita Mall, McCullough Building, Room 246, Stanford, CA 94305-4045, USA.
Email: heilshorn@stanford.edu

Funding information
American Heart Association, Grant/Award Numbers: 903771, 20IPA35310731, 20IPA35360085; Department of Veteran Affairs, Grant/Award Numbers: 1I01BX002310, 1I01BX004259, RX001222; National Institutes of Health, Grant/Award Numbers: R21 NS114549, R01 EB027171, R01 EB027666, R01 HL127113, R01 HL142718, R01 HL151997; National Science Foundation, Grant/Award Numbers: 1829534, CBET 2033302, DMR 2103812

Abstract

Mechanical cues from the extracellular matrix (ECM) regulate vascular endothelial cell (EC) morphology and function. Since naturally derived ECMs are viscoelastic, cells respond to viscoelastic matrices that exhibit stress relaxation, in which a cell-applied force results in matrix remodeling. To decouple the effects of stress relaxation rate from substrate stiffness on EC behavior, we engineered elastin-like protein (ELP) hydrogels in which dynamic covalent chemistry (DCC) was used to crosslink hydrazine-modified ELP (ELP-HYD) and aldehyde/benzaldehyde-modified polyethylene glycol (PEG-ALD/PEG-BZA). The reversible DCC crosslinks in ELP-PEG hydrogels create a matrix with independently tunable stiffness and stress relaxation rate. By formulating fast-relaxing or slow-relaxing hydrogels with a range of stiffness (500–3300 Pa), we examined the effect of these mechanical properties on EC spreading, proliferation, vascular sprouting, and vascularization. The results show that both stress relaxation rate and stiffness modulate endothelial spreading on two-dimensional substrates, on which ECs exhibited greater cell spreading on fast-relaxing hydrogels up through 3 days, compared with slow-relaxing hydrogels at the same stiffness. In three-dimensional hydrogels encapsulating ECs and fibroblasts in coculture, the fast-relaxing, low-stiffness hydrogels produced the widest vascular sprouts, a measure of vessel maturity. This finding was validated in a murine subcutaneous implantation model, in which the fast-relaxing, low-stiffness hydrogel produced significantly more vascularization compared with the slow-relaxing, low-stiffness

hydrogel. Together, these results suggest that both stress relaxation rate and stiffness modulate endothelial behavior, and that the fast-relaxing, low-stiffness hydrogels supported the highest capillary density in vivo.

KEYWORDS
endothelial cell, hydrogel, stiffness, stress relaxation, vascular sprouting

1 | INTRODUCTION

Vascular endothelial cells (ECs) line the inner layer of blood vessels, and they play key roles in physiological and pathological context. ECs interact with circulating blood elements and regulate vascular homeostasis.[1,2] In conditions of ischemic cardiovascular diseases associated with peripheral arterial disease or heart failure, the ECs initiate the formation of new blood vessels through angiogenesis. In addition, for creating scalable engineered tissues in which vascularization is essential, the ECs are also an important driver of vascularization. Since ECs respond to microenvironmental cues, including those from the extracellular matrix (ECM), it is critical to understand how ECM properties affect endothelial behavior.

The ECM microenvironment mediates the response of vascular ECs to form new vasculature through biomolecular and physical cues. Previous studies from our group and others have demonstrated that cell-adhesive ligands and mechanical properties differentially regulate cellular responses such as cell migration, proliferation, differentiation, dedifferentiation, and apoptosis.[3–13] ECMs within the human body are viscoelastic rather than purely elastic, and cells respond to matrix viscoelasticity.[14–16] Naturally derived ECMs exhibit stress relaxation, in which a cell-applied force results in matrix remodeling, leading to the relaxation of cell-imposed stress. However, this matrix cue has not been widely studied in EC cultures due to a lack of biomaterials that enable careful tuning of stress relaxation rate without concomitant alteration of other matrix cues such as stiffness.

In this contribution, we developed hydrogels with independently tunable stress relaxation rate and stiffness properties and studied their effects on EC behavior. To do this, we engineered elastin-like protein (ELP) hydrogels that contain the pentapeptide repeat Val-Pro-Gly-Xaa-Gly amino acid sequences derived from tropoelastin, where Xaa can be any amino acid except Pro.[17] The structure of ELP allows for the control of the cell-adhesive ligand type and density of the material without changing its mechanical properties. In addition, ELPs are cytocompatible, biodegradable, and undergo a lower critical solution temperature (LCST) phase transition, which facilitates their purification.[18]

To form ELP hydrogels, dynamic covalent chemistry (DCC) crosslinking is used between hydrazine-modified ELP (ELP-HYD) and aldehyde- or benzaldehyde-modified polyethylene glycol (PEG-ALD or PEG-BZA, respectively). The stiffness of the ELP-PEG hydrogels is controlled by modifying the concentration of ELP and PEG components, which tunes the total number of crosslinks. Separately, the stress relaxation rate is controlled by selecting either the PEG-ALD or PEG-BZA variant, since the aldehyde and benzaldehyde groups are known to have different reaction kinetics with the hydrazine functional group.[19] These tunable mechanical properties of the hydrogel make ELP-based matrices attractive for studying EC behavior in well-controlled biomechanical environments.[18] The reversible DCC crosslinking bonds in ELP-PEG hydrogels create a stress-relaxing hydrogel and allow the embedded cells to remodel the hydrogel by applying cellular forces.[20] Previous work by Chaudhuri et al.[15] showed that stress relaxation can independently modulate the response of other cell types like mesenchymal cells, such that their spreading, proliferation, and osteogenic differentiation is enhanced in fast-relaxing hydrogels. Here, we studied the role of substrate stiffness and stress relaxation rate in modulating EC responses, including attachment, proliferation, sprouting, and in vivo vascularization. Our results suggest that these two mechanical cues have differential effects on endothelial behavior.

2 | MATERIALS AND METHODS

2.1 | Elastin-like protein expression and purification

ELP (Figure 1A)[18] was expressed and purified using standard recombinant protein technology.[21] Briefly, protein sequences were cloned into pET15b plasmids, expressed in *Escherichia coli* (strain BL21[DE3]) and then induced with 1 mM isopropyl b-d-1-thiogalactopyranoside (IPTG) at an OD_{600} of 0.8. After 7 h, the harvested cell pellets were suspended, lysed by three freeze–thaw cycles, and purified by iterative inverse temperature-cycling. Protein molecular weight and purity were confirmed by sodium dodecyl sulfate polyacrylamide gel electrophoresis (SDS-PAGE). Purified ELP was dialyzed for 3 days (10,000 MWCO, 4°C, deionized water) to desalt. The ELP was then lyophilized.

2.2 | Synthesis and characterization of ELP-hydrazine

ELP (MW: 37840, 300 mg) was dissolved in 4.1 mL anhydrous dimethyl sulfoxide (DMSO) and 4.1 mL anhydrous dimethylformamide (DMF). Separately, tri-Boc hydrazinoacetic acid (90.83 mg, 0.232 mmol, 2.1 equiv. per amine, 390.43 g/mol), Hexafluorophosphate Azabenzotriazole Tetramethyl Uronium (84.24 mg, 0.221 mmol, 2.0 equiv. per amine, 380.23 g/mol), and 4-methylmorpholine (61.35 µL, 0.558 mmol, 5.0 equiv. per amine, 101.15 g/mol, 0.92 g/mL) were dissolved in

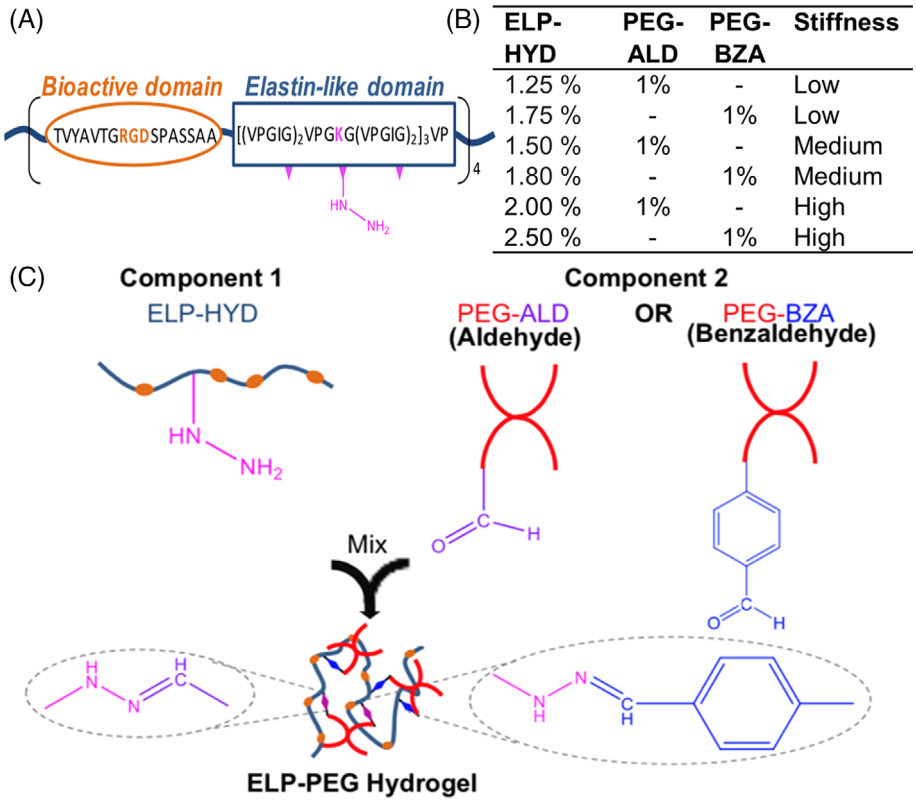

FIGURE 1 ELP-PEG hydrogel synthesis. (A) ELP structure showing RGD cell-adhesive ligand and elastin-like domains (reproduced from[18]). (B) Table of hydrogel formulations formed by the mixing of ELP-HYD, PEG-ALD, and PEG-BZA at varying concentrations to achieve low-, medium-, or high-stiffness hydrogels with either PEG-ALD or PEG-BZA to form fast and slow stress relaxation rates, respectively. (C) Schematic of mixing ELP-HYD with PEG-ALD or PEG-BZA to obtain ELP-PEG hydrogel.

4.1 mL anhydrous DMF. The reaction was stirred for 5 min, and then the ELP solution was added, and the reaction was allowed to proceed overnight at room temperature. The product was precipitated in ice-cold diethyl ether, dried, and treated with a solution of 2.5% triisopropylsilane in 50:50 dichloromethane (DCM):trifluoroacetic acid for 4 h to remove the Boc group. The resulting compound was precipitated in ice-cold diethyl ether, dissolved in deionized water, dialyzed for 3 days (10,000 MWCO, 4°C, deionized water), and lyophilized. To quantify the modification efficiency, samples before the removal of Boc groups were assessed by ^{1}H NMR spectroscopy (Varian Inova, 500 MHz) using deuterated DMSO as a solvent. The modification efficiency was determined by comparing the integration of methyl protons on the Boc group with the aromatic protons of tyrosine in Boc-protected ELP-HYD (Figure S1).

2.3 | Synthesis of PEG-aldehyde and PEG-benzaldehyde

PEG-aldehyde (PEG-ALD) was synthesized via a copper-mediated click-chemistry reaction by dissolving 10 kDa, 8-arm PEG-Alkyne (Creative PEG Works) in isotonic 10× phosphate-buffered saline (PBS) buffer at 10 mg/mL. Simultaneously, copper sulfate (6.0 mg in 10 mL, 2.4 mM) and sodium ascorbate (89.5 mg in 10 mL, 45.2 mM) were dissolved in deioinized H_2O, and the solutions were purged in N_2 gas for 30 min. Immediately after, sodium ascorbate (4.5 mM), copper sulfate (2.4 mM), and azido-PEG3-ALD (BroadPharm) (2 equiv. per alkyne) in DMSO (500 μL) were added to the PEG solution in sequential order. The reaction was purged for an additional 10 min and then covered and left to react overnight before carrying out dialysis and concentrating via lyophilizing.

PEG-benzaldehyde (PEG-BZA) was synthesized via an amidation reaction between 10 kDa, 8-arm PEG-NH_2 (Creative PEG Works) and 4-formylbenzoic acid (Sigma). Briefly, 8-arm PEG-NH_2 was dissolved in anhydrous DCM before adding 4-formylbenzoic acid (2 equiv. per NH_2). After the solution had stirred for 10 min, 1-ethyl-3-[3-dimethylaminopropyl]carbodiimide hydrochloride (EDC) (2 equiv. per 4-formylbenzoic acid) was added to the reaction and left to stir overnight. The reaction was then precipitated in cold diethyl ether and collected by centrifugation. The collected material was then vacuum-dried before dialysis and concentrated via lyophilizing. Both PEG-ALD (∼5.7 motifs per PEG) and PEG-BZA (∼4.8 motifs per PEG) were characterized by NMR in CD_2Cl_2 and D_2O, respectively (Figure S2).

2.4 | Formation of ELP-PEG hydrogels

ELP-PEG hydrogels of varying formulations (Figure 1B) were prepared by simple mixing of ELP-HYD with PEG-ALD or PEG-BZA (Figure 1C). ELP-HYD was dissolved in PBS at 4°C. PEG-ALD and PEG-BZA solutions were diluted to 2% (w/v) in PBS and kept on ice. To make the hydrogels, ELP-HYD of different concentrations were thoroughly mixed with either PEG-ALD or PEG-BZA, avoiding any bubble formation. The hydrogels were incubated on ice for 5 min, at room temperature for 15 min, and then at 37°C for 10 min.

2.5 | Hydrogel mechanical characterization

Hydrogel formulations were crosslinked in situ on an ARG2 rheometer (TA Instruments) using a 20-mm diameter cone-plate geometry. All tests were conducted with 50-μL samples and a humidity chamber to prevent sample dehydration. To mimic gelation conditions for cell culture, the hydrogel components were allowed to react at 1% strain and 1 rad/s oscillatory frequency for 5 min at 4°C followed by 15 min at 25°C and 15 min at 37°C. This protocol was followed by a frequency sweep from 0.1 to 100 rad/s at 1% constant strain to obtain storage (G') and loss (G'') moduli. The storage and loss moduli were taken to be the values at 1 rad/s from these measurements. Three independent samples were measured and averaged as a representative matrix stiffness. For stress relaxation measurements, a 10% step strain was then applied, and the stress relaxation response was measured for at least 60 min. Shear-thinning properties of the hydrogel samples were characterized by measuring the viscosity at alternating low (0.1 s^{-1}) and high (10 s^{-1}) strain rates for 30 s each at 37°C.

2.6 | Characterization of ELP-PEG aggregate formation using coherent anti-Stokes Raman scattering microscopy

We characterized the microstructure of the ELP-PEG hydrogels in situ by collecting density maps of carbo-hydrogen (CH) vibrations using coherent anti-stokes raman scattering (CARS) microscopy at 37°C in a microscope incubator (Okolab stage top) mounted on an inverted microscope (Ti2-E with a C2 confocal scanning head and a Nikon CFI Apochromat TIRF 100XC Oil objective, NA = 1.49). The CH vibrations were coherently driven by two laser beams overlapped in time and space, generated by a picosecond-pulsed laser system consisting of a 1031 nm fiber laser and an optical parametric oscillator (OPO) tunable between 690–960 nm (APE picoEmerald S, 2 ps pulse length, 80 MHz repetition rate, and 10 cm^{-1} bandwidth). We have previously observed protein-specific stretching modes of CH_3 for ELP in the range 2930–2940 cm^{-1}, and to address this vibration the OPO wavelength was set to 791 nm.[11,18,22–25] The CARS signal depends quadratically on the number density of the probed vibrational group, providing contrast for regions dense in ELP polymer without the need for external labels or other disruptive sample preparations. Furthermore, the penetration depth of the near-infrared excitation beams and the automatic optical confocal sectioning of the third-order CARS process enable probing of the three-dimensional (3D) structure at high resolution deep inside the hydrated ELP-PEG gels. For all CARS imaging in this work, the excitation powers at the sample were 27 mW for the OPO beam and 13 mW for the 1031 nm Stokes beam, and CARS signals were collected in the forward direction using a photomultiplier tube (Hamamatsu, R6357) with 10.8 μs dwell time.

For the acellular 3D scaffolds, we collected Z-stacks (covering a 32-μm field of view and a depth of 6 μm) with 31 nm pixel size and 0.25 μm vertical separation between adjacent z-positions. The acquired images were prepared and analyzed in ImageJ. Each slice was normalized through a nonresonant CARS reference image generated from the coverslip. After shadow correction, the images were bandpass Fourier filtered between 1 and 1024 pixels with 5% tolerance of direction for the suppression of horizontal stripes, followed by a gaussian blur filter (sigma = 3) and background subtraction with a rolling ball radius of 50 pixels. The gel porosity was then extracted by calculating the percentage of voxels with zero value after Otsu thresholding. The size distribution of the ELP-PEG polymer-dense regions was evaluated by the local thickness plug-in (masked, calibrated, silent). The ratio of the average, nonprocessed signal in the polymer-dense regions (identified by the thresholding routine described above) over the surrounding signal was used as an empirical measure of the packing density of ELP-PEG polymers (n = 4). An overview of the workflow for evaluating the CARS data is presented in Figure S3.

2.7 | Cell culture

To model EC response in ELP-PEG hydrogels, primary human umbilical vein ECs (HUVECs, Angio Proteomie) with green fluorescence protein (GFP) reporter were selected because they are well-characterized and the most widely used type of ECs for in vitro EC research,[26] which may be beneficial for reproducibility of findings. The HUVECs were cultured in endothelial cell growth medium (EGM-2MV, Lonza) containing 2% fetal bovine serum, vascular endothelial growth factor, human fibroblast growth factor, insulin growth factor (R3-IGF-I), human epidermal growth factor, hydrocortisone, ascorbic acid, and heparin. Primary human dermal fibroblasts (HNDFs, Angio Proteomie) with red fluorescence protein tag were cultured in Dulbecco's Modified Eagle Medium (DMEM, Gibco) supplemented with 10% fetal bovine serum and 1% penicillin/streptomycin.

2.8 | Endothelial culture on 2D ELP-PEG hydrogels

In 96-well plates, 10 μL of varying hydrogel formulations in Figure 1B was prepared and deposited. GFP-labeled HUVECs (3.1×10^3 cells/cm^2) were seeded on top of the hydrogels and cultured for up to 2 weeks. Cells were imaged using confocal microscopy for up to 14 days. A recursive thresholding algorithm was developed in MATLAB R2018b (MathWorks, Inc.) to identify the cells in the images and to quantify number of attached cells and surface area in each condition. The cell area was calculated by multiplying the pixel surface area by the number of pixels occupied by the cell, which had values above a decided threshold. The data was averaged over ≥38 individual cell area values per hydrogel formulation at each time point (n = 3).

2.9 | Cell encapsulation into 3D ELP-PEG hydrogels

ELP-HYD and PEG-ALD/PEG-BZA solutions were prepared and placed on ice. ELP-HYD solutions with six different concentrations were

prepared according to Figure 1B. The ELP-HYD solutions were mixed with 1% (w/v) PEG-ALD or PEG-BZA to fabricate hydrogels with tunable mechanical elastic moduli or stress relaxation properties. To house the 3D gels, custom-made 4-mm diameter silicone molds were immobilized onto glass coverslips by oxygen plasma treatment and then placed into 24-well dishes. Into each mold, 5 µL of PEG-ALD or PEG-BZA solution was added and uniformly dispersed across the mold using a pipette tip. GFP-HUVECs and RFP-HNDFs were dissociated by TrypLE (Invitrogen), pelleted by centrifugation, and then resuspended in ELP-HYD. 5 µL of the ELP-HYD component with cells was then added to the PEG-ALD or PEG-BZA component and mixed by swirling with the pipette tip. The total cell density was kept constant at 10×10^6 cells/mL at a 1:1 ratio of GFP-HUVEC to RFP-HNDF. The hydrogels were incubated on ice for 5 min, at room temperature for 15 min, and subsequently at 37°C for 10 min. After gelation, EGM2-MV growth medium was added to each well and exchanged every 2 days. After 14 days, confocal images were captured to evaluate cell morphology using confocal fluorescence imaging (Zeiss, LSM710). The branch lengths were measured as the distance from one branch point to the next closest branch point, and the branch width measured the average width per branch. The branch lengths and widths were averaged based on $n = 3$ samples using ImageJ software.

2.10 | ELP-PEG effects on vascularization in subcutaneous murine model

To compare the effects of stress relaxation rate on vascularization in vivo, a 1:1 coculture of tagged HUVEC/HDNF (a total of 10^6 cells) was mixed in the low-stiffness hydrogels with either fast or slow relaxation rates, before injecting 30 µL of hydrogel subcutaneously using a 28-G needle into NOD SCID mice. After 14 days, the hydrogels were explanted along with the local muscle and skin for frozen sectioning and immunofluorescence staining of capillary density. The capillary density of the subcutaneous region was visualized using a rat antimouse CD31 antibody (BD). The tissue sections were fixed in 4% paraformaldehyde, permeabilized in 0.1% Triton-X100, blocked in 1% bovine serum albumin, and then incubated with the CD31 antibody.[27,28] After 24 h of incubation at 4°C, the tissue sections were washed in PBS and then incubated with an Alexafluor-488-conjugated secondary antibody. Total nuclei were stained using Hoechst33342. The vessels were identified by a single layer of CD31-expressing cells that was greater than that of the size of a cell nucleus.[29,30] To quantify microvascular density in the subcutaneous space, the number of spatially separate $CD31^+$ vessels was counted and normalized to the area of the subcutaneous space ($n = 3$). All animal studies were approved by the Institutional Animal Care and Use Committee at the Veterans Affairs Palo Alto Health Care System.

2.11 | ELP-PEG hydrogel degradation in vivo

To quantify the degradation of ELP-PEG hydrogels in vivo, fluorescently labeled protein-engineered hydrogels fabricated from ELP-HYD modified with tyrosine selective 4-phenyl-3H-1,2,4-triazoline-3,5(4H)-dione azide (PTAD-AZ)[31] were conjugated with sulfonated-cyanine 5 (Cy5) via click-chemistry to yield ELP-HYD-Cy5. The fluorescent ELP was mixed at a 1:10 ratio with nonfluorescent ELP-HYD before encapsulating 10^6 HUVECs and HDNFs at a 1:1 ratio and then injecting subcutaneously in the abdomen of SCID mice. The intensity of the resulting fluorescently labeled ELP-PEG hydrogel was noninvasively quantified over the course of 14 days in the mice using IVIS-200 (Xenogen) fluorescence imaging equipment.

2.12 | Gene expression

To assess the transcriptional changes resulting from hydrogel mechanics, low- and medium- stiffness 3D hydrogels composed of fluorescently tagged HUVEC and HNDF (Figure 1B) were dislodged after 14 days from the silicone mold and directly transferred to TRIzol lysis reagent. The hydrogels were disrupted by sonication (100% amplitude, 0.5 s cycles). Phenol-chloroform extraction was used to isolate RNA, and RNA concentration was measured using a UV–Vis spectrophotometer (NanoDrop 2000, Thermo Scientific). The cDNA was synthesized from total RNA using the Superscript II reverse transcriptase kit (Life Technologies) and a compact thermal cycler (T100 Thermal cycler, Bio-Rad). Gene expression analysis was performed using quantitative real-time polymerase chain reaction (RT-PCR). RT-PCR was performed using Taqman primers encoding the following genes: hepatocyte growth factor (HGF), platelet derived growth factor (PDGF), basic fibroblast growth factor (FGF-2), vascular endothelial growth factor-1, angiogenin, and GAPDH (all from Thermo Fisher Scientific). qPCR was performed (7900HT Sequence Detection System, Applied Biosystems). Using GAPDH as a housekeeping gene, the normalized relative gene expression was determined using the ΔΔCT method.[32]

2.13 | Statistical analysis

Data are shown as mean ± standard deviation. For comparisons of two groups, a Student's *t*-test was performed. For three or more treatment groups, a one-way analysis of variance (ANOVA) was performed using Tukey multiple comparisons testing. For analysis of repeated samplings of the same treatment group, a repeated measures ANOVA was performed with Tukey multiple comparisons testing. Statistical significance was accepted at $p < .05$. Statistical analysis was performed using Prism (GraphPad) software.

3 | RESULTS

3.1 | Tuning ELP-PEG hydrogel mechanical properties

A new family of protein-engineered hydrogels was fabricated from ELP and PEG. Recombinantly expressed ELP consists of alternating

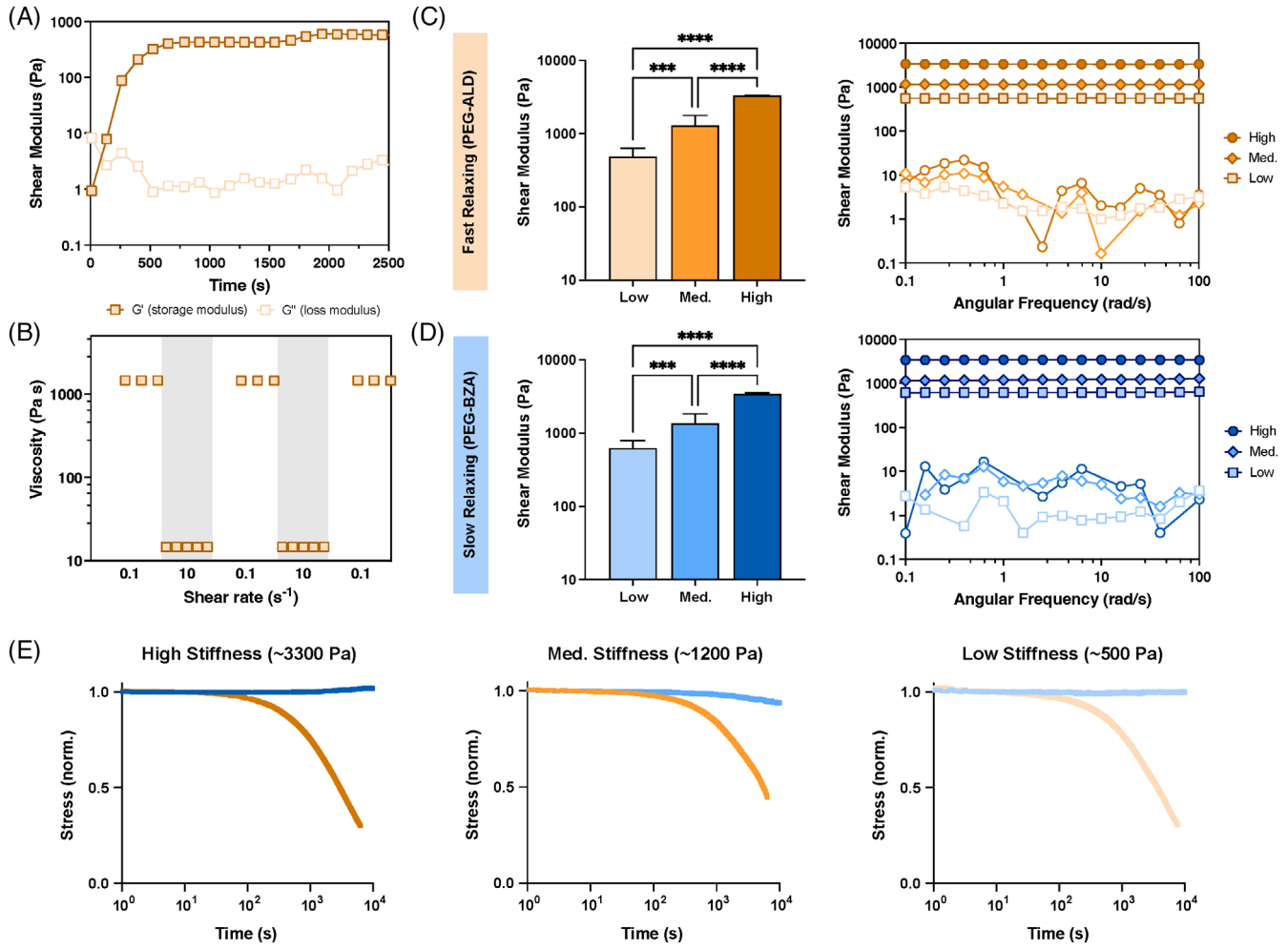

FIGURE 2 Characterization of ELP-PEG hydrogel rheological properties. (A) Representative gelation time sweep of an ELP-PEG hydrogel (1.25% ELP-HYD, 1% PEG-ALD) showing storage moduli (G', filled symbols) and loss moduli (G'', open symbols) during crosslinking. (B) Shear-thinning and recovery behavior of an ELP-PEG hydrogel under alternating shear rates of 0.1 and 10 s^{-1} at 37°C. (C, D) Left panels: Average shear storage moduli (G') of ELP-PEG hydrogels ($n = 3$). Right panels: Representative frequency sweeps performed at a fixed strain of 1% showing storage moduli (G', filled symbols) and loss moduli (G'', open symbols) for all gel formulations. Labels refer to formulation names as described in Figure 1B. Gels formed with PEG-ALD are shown in (C), and PEG-BZA are shown in (D). (E) Representative stress relaxation curves comparing fast-relaxing (PEG-ALD) and slow-relaxing (PEG-BZA) hydrogels for all gel formulations. ***$p < .001$, ****$p < .0001$.

sequences of elastin-derived and fibronectin-derived peptides.[33] Specifically, cell–matrix interactions are maintained through the integrin-binding peptide RGD to promote the adhesion of encapsulated cells (Figure 1). ELP was functionalized with a hydrazine group, whereas the PEG was functionalized with an aldehyde group to result in a hydrazone-crosslinked hydrogel through DCC (Figure 2). A thermal phase transition provides secondary crosslinking, owing to the LCST of ELP (~32°C).[22]

The ELP-PEG material system allows for independent tuning of various matrix mechanical properties, allowing for careful study of how HUVECs respond to changes in matrix stiffness and stress relaxation rate. Matrix stiffness was tuned by varying the weight percent of the ELP component, while keeping a constant weight percent of PEG. Independent from stiffness, matrix stress relaxation rate was tuned by altering the crosslinking moiety functionalized to the PEG component, in which an aliphatic aldehyde (PEG-ALD) yielded fast stress-relaxing gels whereas a benzaldehyde (PEG-BZA) yielded slow stress-relaxing gels. First, we demonstrated that the ELP-PEG gels undergo gelation and reached a plateau modulus within 30 min after mixing (Figure 2A). Once the two hydrogel components were combined, the solution temperature was incrementally raised, starting initially at 4°C for 5 min, then 25°C for 15 min, and finally 37°C for 10 min. This rapid gelation using cyto-compatible temperatures renders the ELP-PEG gels well-suited for cell encapsulation. Additional oscillatory rheological studies confirmed that the hydrogels exhibit shear-thinning properties by assessing hydrogel viscosity at low (0.1 s^{-1}) and high (10 s^{-1}) shear rates. At high shear rates, the viscosity rapidly decreased to ~15 Pa·s and recovered to the original viscosity of ~1400 Pa·s at low shear rates (Figure 2B). Fully reversible shear-thinning and rapid hydrogel recovery behavior across multiple cycles facilitates facile extrusion through a syringe.

With these rheological properties in mind, we created a family of ELP-PEG hydrogels, which we refer to as hydrogels of low-

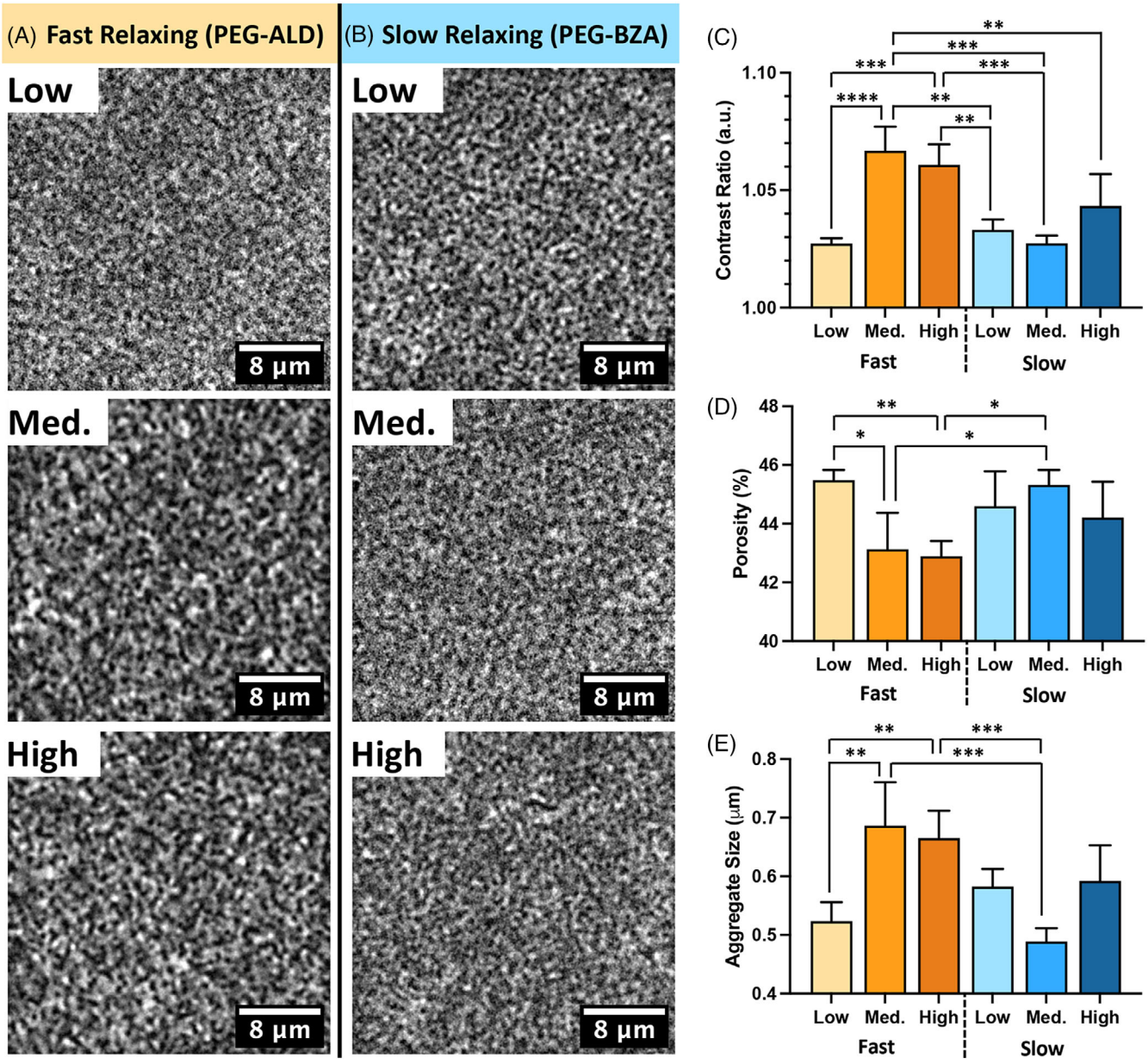

FIGURE 3 ELP-PEG hydrogel microstructure from CARS microscopy. Representative CARS images at 2940 cm^{-1} of the (A) fast-relaxing and (B) slow-relaxing ELP-PEG gels with different stiffness. For each gel, the contrast ratio (C) of polymer-dense regions versus background, the porosity (D) by fraction of pixels below the threshold level, and the size (E) of polymer aggregate diameter were evaluated ($n = 4$). *$p < .05$, **$p < .01$, ***$p < .001$, ****$p < .0001$. Scale bar: 8 μm.

(~500 Pa), medium- (~1.2 kPa), and high- (~3.3 kPa) stiffness (Figure 2C,D). This range in stiffness values was consistent with the range of reported values for EC stiffness (~0.5–4 kPa).[6,34–37] To achieve stiffness-matched hydrogel conditions, we modified the ELP concentration for the gels containing PEG-ALD and the gels containing PEG-BZA. Due to differences in equilibrium constants for the respective crosslinking reactions,[38] it was necessary to modify the concentration of ELP to achieve the same elastic modulus when substituting the aliphatic aldehyde for the benzaldehyde (Figure S4). We next evaluated the stress relaxation properties of the ELP-PEG hydrogels. Under a constant, applied strain, the gels containing PEG-BZA at all stiffness conditions exhibit a minimal decrease in stress over the course of 2.5 h, whereas the hydrogels containing PEG-ALD dissipated their stress much more rapidly, resulting in fast relaxation (Figure 2E). Based on this characterization, for simplified nomenclature, we refer to hydrogels containing PEG-ALD as "fast-relaxing" hydrogels, whereas those containing PEG-BZA are regarded as "slow-relaxing" hydrogels.

To further evaluate how the ELP-PEG formulations aggregate into a mesh of polymer-dense regions and pores, we characterized the hydrogel microstructure by CARS microscopy (Figure 3). This technique visualizes molecular assemblies by targeting vibrational modes

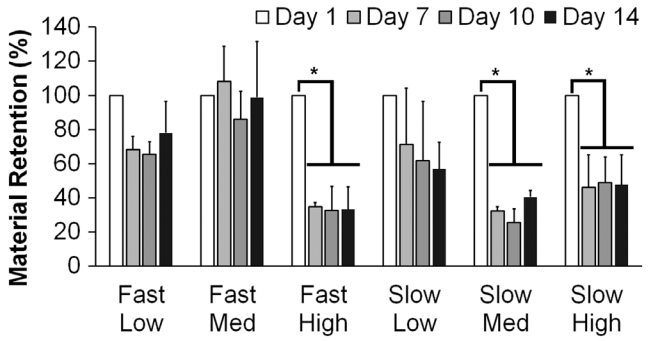

FIGURE 4 Hydrogel retention after in vivo subcutaneous injection of encapsulated HUVECs and HNDFs. The hydrogels were conjugated with near-infrared dye. Noninvasive, fluorescence imaging quantification of material retention relative to day 1, for up to 14 days after transplantation by injection ($n = 3$). *$p < .05$.

that are coherently driven by the difference in frequency, Ω, between two excitation laser beams. We tuned Ω to 2940 cm^{-1}, which targets CH_3 stretching modes and provides good contrast for the ELP-PEG polymer aggregates. Since the CARS signal is quadratically dependent on the number density of the probed molecules, we used the contrast ratio between the signal from polymer aggregates relative to the background signal from the pores as an empirical measure of the ELP-PEG packing density (Figure 3C). We further evaluated the gel porosities by determining the volume percentage occupied by the pores, which reflects the volume excluded by the thresholding approach (see Methods) divided by the total volume of the probed gel (Figure 3D). The aggregate sizes were then determined by measuring the average diameter of the polymer dense regions (Figure 3E). Across these parameters, the fast-relaxing (PEG-ALD) gels with medium and high stiffness formulations stand out as the hydrogels with higher contrast ratio and aggregate size, but with lower porosity, when compared with the other gels. Despite these statistically significant differences, the absolute range of gel porosity was narrow, ranging from 43% to 46% (Figure 3D), while ELP aggregate size ranged from 0.5 to 0.7 μm (Figure 3E). Comparing the two ELP-PEG gels with low stiffness showed no statistically significant differences between any of the gel microstructure parameters for the fast-relaxing and slow-relaxing gels. Similarly, in comparing the two ELP-PEG gels with high stiffness, there were no statistically significant differences between any of the gel microstructure parameters for the fast-relaxing and slow-relaxing gels.

Together, these data demonstrate that ELP-PEG hydrogels with similar microstructure could be successfully engineered with independently tunable stiffness and stress relaxation rate, as well as gelation conditions amenable to cell encapsulation. As a result, this mechanically tunable family of hydrogels could be used to study the effects of stiffness and stress relaxation rate on EC behavior.

3.2 | Degradation of ELP-PEG hydrogel in vivo

To study the retention of the ELP-PEG hydrogels, we chose an in vivo model because it better reflects hydrogel biodegradation in biological contexts. To track the degradation, we employed fluorescently labeled ELP-PEG to produce low-, medium-, and high-stiffness gels. Each hydrogel formulation was used to encapsulate HUVECs:HDNFs at a 1:1 ratio before injecting subcutaneously into the abdominal region of SCID mice. As shear-thinning gels that reversibly regain their original viscosity, the ELP-PEG hydrogels were easily injectable using a 28-G needle, while forming a palpable hydrogel at the site of injection. For the fast-relaxing hydrogels, the material with high stiffness showed the greatest biodegradability, with statistically significant reduction in fluorescence intensity at 14 days to 33% ± 13%, relative to day 1 (Figures 4 and S5). For the slow-relaxing hydrogels, the high-stiffness and medium-stiffness matrices both experienced significant biodegradation at 14 days (48% ± 17% and 40% ± 4%, respectively). At 14 days, the fluorescence intensity signaled more retention in the low-stiffness formulations for both fast-relaxing (78% ± 1%) and slow-relaxing (57% ± 15%) gels. The fast-relaxing, medium-stiffness formulation had the highest retention (99% ± 33%) after 14 days. These results suggest that the high-stiffness hydrogels were more prone to biodegradation, and that 33%–99% of the six different hydrogel formulations persisted over the course of 14 days.

3.3 | 2D ELP-PEG hydrogel effects on EC attachment and proliferation in vitro

To study the effects of stiffness and stress relaxation rate on HUVECs, we first examined cell proliferation and attachment on top of 2D hydrogel formulations composed of low-, medium-, and high-stiffness having either fast or slow stress relaxation rates. Over the course of 2 weeks, the number and morphology of GFP-tagged ECs were quantitatively assessed non-invasively by fluorescence imaging. Although cell numbers were not statistically different among the various hydrogel formulations over time (Figure S6), the morphology and spreading area showed distinctive differences. Since HUVECs are known to undergo cell–cell contact inhibition upon confluency, their morphology was quantitatively assessed over the course of 7 days, during which the cells remained subconfluent. As a general trend, when comparing cell spreading on fast-relaxing versus slow-relaxing hydrogels at the same stiffness, the HUVECs had greater cell spreading on faster relaxing matrices (Figure 5). Initially at 1.5 h after cell seeding, the fast-relaxing hydrogel at medium stiffness supported an average cell spreading area of 2124 ± 134 μm^2, compared with that on slow-relaxing, medium-stiffness hydrogels (1242 ± 171 μm^2), representing 70% greater cell spreading on fast-relaxing hydrogels ($p < .05$). Similarly at 1.5 h, on fast-relaxing, high-stiffness hydrogels, the average spreading area (2641 ± 495 μm^2) was 65% higher than on slow-relaxing hydrogels (1695 ± 111 μm^2) ($p < .05$). The significantly higher cell spreading area on fast-relaxing, high-stiffness hydrogels, compared with on slow-relaxing hydrogels, was maintained after 1 and 3 days of cell attachment ($p < .05$). Besides stress relaxation differences, we also observed stiffness effects. At 1.5 h after cell attachment, the cell spreading area was significantly higher on slow-relaxing hydrogels with low stiffness (2147 ± 318 μm^2), compared with

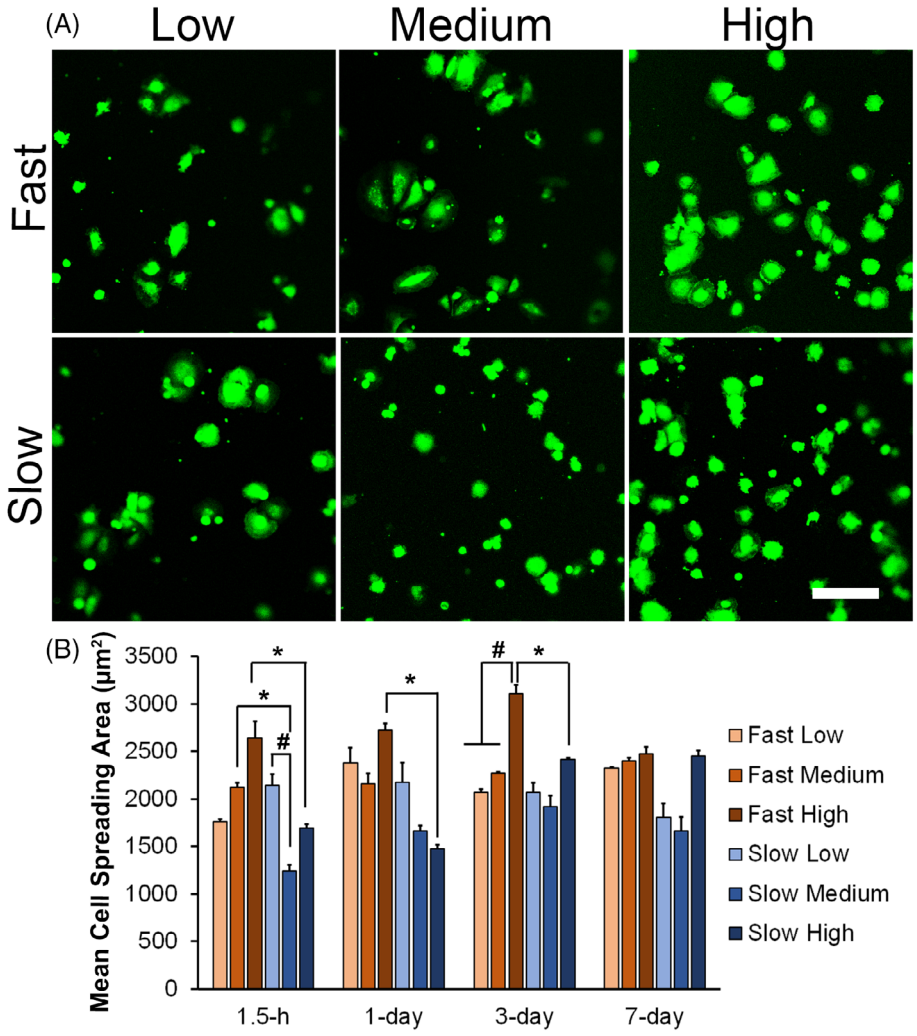

FIGURE 5 Effects of stress relaxation rate and stiffness on endothelial cell spreading area. (A) Representative fluorescent images of GFP-tagged HUVECs at 1.5 h after initial seeding onto hydrogels. (B) Mean cell spreading area over time. The data was averaged over ≥38 individual cell area values per hydrogel formulation at each time point ($n = 3$). $^{*}p < .05$ denotes statistically significant comparisons of samples with different stress relaxation rates. $^{\#}p < .05$ denotes significant comparisons of samples with different stiffness. Scale bar: 200 μm.

medium-stiffness (1242 ± 171 μm^2) hydrogels ($p < .05$). Interestingly, for fast-relaxing hydrogels, there was the opposite finding after 3 days in which cell surface area correlated with increasing substrate stiffness (fast, low: 2071 ± 77 μm^2; fast, medium: 2271 ± 38 μm^2; fast, high 3104 ± 262 μm^2; $p < .05$). These results show that endothelial morphology was affected by both stress relaxation rate and stiffness on 2D substrates.

3.4 | 3D ELP-PEG hydrogel effects on vascular sprouting in vitro

Since vascularization is an important functional characteristic of HUVECs, we next sought to assess the effects of stress relaxation rate and stiffness on vascular sprouting within 3D ELP-PEG hydrogels. Compared with on their own, ECs are known to form more stable tube-like structures in 3D hydrogels when cocultured with support cells such as fibroblasts.[39,40] Therefore, we embedded GFP-tagged HUVECs with RFP-tagged HDNFs at a 1:1 ratio within 3D hydrogels that were cast into custom-made microwells. After 14 days, vascular sprouting was observed only in the groups consisting of fast-relaxing, low-stiffness hydrogels, fast-relaxing, medium-stiffness hydrogels, and slow-relaxing, low-stiffness hydrogels (Figure 6A). By contrast, the cells in all high-stiffness hydrogels as well as the slow-relaxing, medium-stiffness hydrogel remained primarily rounded. By measuring the branch lengths that span one branch point to the next branch point (Figure 6B), we determined that the fast-relaxing, low-stiffness hydrogel (113 ± 75 μm) supported significantly shorter branch lengths than the fast-relaxing, medium-stiffness hydrogel (181 ± 125 μm) but had significantly longer branch lengths than the fast-relaxing, high-stiffness hydrogel that did not support branch formation ($p < .0001$). Among the slow-relaxing hydrogels, the low-stiffness ones showed significantly longer branch lengths (85 ± 29 μm) than the medium- or high-stiffness hydrogels that did not support sprouting ($p < .0001$). Stress relaxation effects were also observed in which the fast-relaxing, medium-stiffness hydrogels showed significantly longer branch lengths (181 ± 125 μm) compared with the slow-relaxing, medium-stiffness hydrogels that did not support branching ($p < .05$).

The branches were significantly wider in the fast-relaxing, low-stiffness hydrogel (22 ± 9 μm) compared with the medium-stiffness hydrogel (18 ± 7 μm) and high-stiffness hydrogel (0 ± 0 μm) ($p < .0001$). The slow-relaxing hydrogels shared a similar relationship

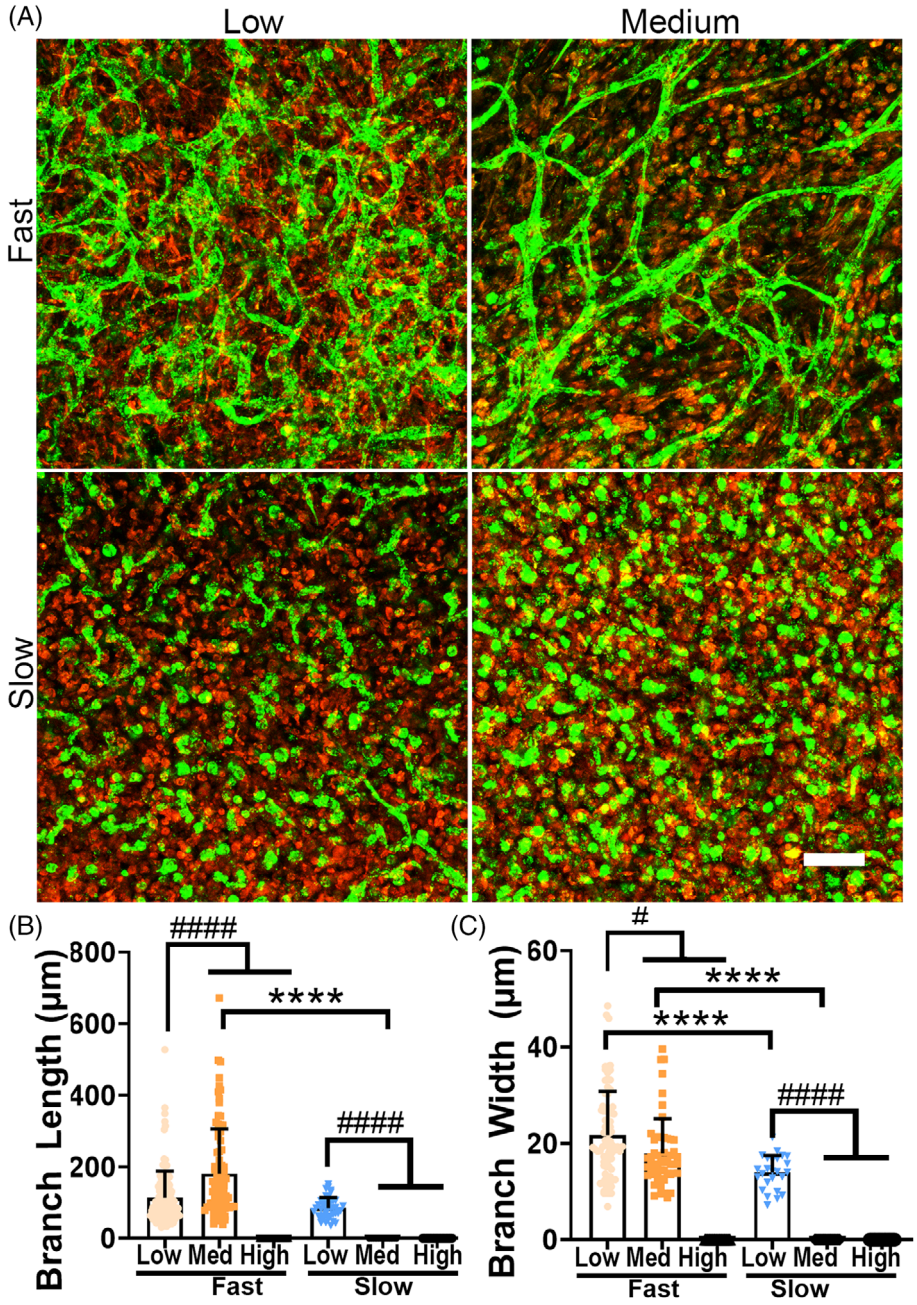

FIGURE 6 Effect of stress relaxation rate and substrate stiffness on vascular sprouting within 3D hydrogels. (A) Representative images of HUVEC and fibroblast cocultures after 14 days. Quantification of mean branch length (B) and branch width (C) after 14 days ($n = 3$). $^{****}p < .0001$ denotes statistically significant comparisons of samples with different stress relaxation rates. $^{\#\#\#\#}p < .0001$ and $^{\#}p < .05$ denote significant comparisons of samples with different stiffness. Scale bar: 200 μm.

in which the low-stiffness hydrogels had significantly wider branches (14 ± 4 μm), compared with the medium-stiffness (0 ± 0 μm) or high-stiffness (0 ± 0 μm) hydrogels ($p < .0001$). These findings suggested that the fast-relaxing, low-stiffness hydrogels promoted wider branches, which is a measure of maturity. Stress relaxation effects were also observed in which the fast-relaxing, medium-stiffness hydrogels showed significantly wider branches (18 ± 7 μm) compared with the slow-relaxing, medium-stiffness hydrogels that did not support branching ($p < .05$). These findings were supported by gene expression analysis in 3D gels showing trends in the upregulation of pro-angiogenic genes (HGF, PDGF, FGF-2) in the fast-relaxing, low-stiffness hydrogels, compared with other formulations, as a potential mechanism by which stress relaxation rates modulate angiogenic responses (Figure S7). These findings show that the fast-relaxing 3D hydrogels support vascular sprouting over a broader range of stiffness, compared with the slow-relaxing hydrogels. In particular, the fast-relaxing, low-stiffness hydrogels promoted the formation of vascular network-like structures, based on the measurements of branch length and width. These data also suggest that the high-stiffness hydrogels were not compatible with vascular sprouting.

3.5 | ELP-PEG effects on vascularization in subcutaneous murine model

Since the low-stiffness hydrogels were most permissive for vascular sprouting in vitro, we compared the efficacy of the low-stiffness hydrogels to form neovasculature in a subcutaneous implantation

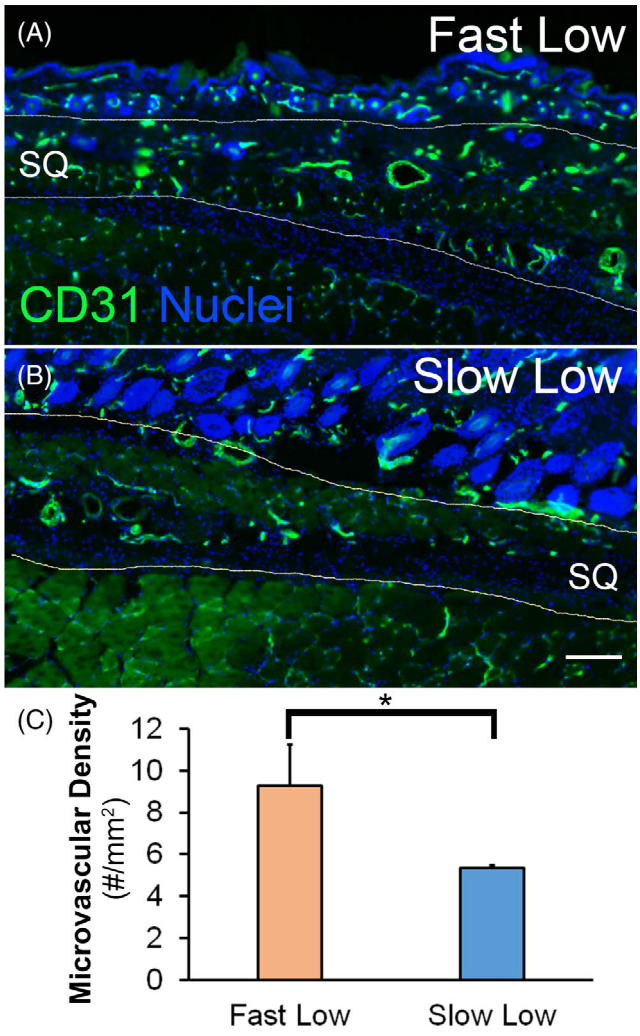

FIGURE 7 Effect of ELP-PEG hydrogel stress relaxation rate on angiogenesis in a subcutaneous model. Representative images of CD31 staining for capillaries in the subcutaneous space for (A) fast-relaxing, low-stiffness hydrogels or (B) slow-relaxing, low-stiffness hydrogels. Dotted lines denote the subcutaneous (SQ) region. (C) Quantification of capillary density ($n = 3$). *$p < .05$. Scale bar: 200 μm.

model. HUVECs and HDNFs were mixed at a 1:1 ratio and then encapsulated into either the fast-relaxing or slow-relaxing hydrogels before injection into NOD SCID mice. After 14 days, we performed immunofluorescence staining for microvessels using a CD31 antibody (Figure 7A,B). Quantification of microvascular density in Figure 7C indicated that the fast-relaxing hydrogel induced significantly more microvessels in the subcutaneous space ($9.3 \pm 2.0/mm^2$) compared with the slow-relaxing hydrogel ($5.4 \pm 0.1/mm^2$) ($p < .05$). These data suggest that the fast-relaxing, low-stiffness hydrogels supported more in vivo vascularization than slow-relaxing, low-stiffness hydrogels.

4 | DISCUSSION

The salient findings from this study are that ELP-PEG hydrogels with tunable stress relaxation rate and substrate stiffness could be successfully generated, and that these mechanical properties differentially modulate EC behavior and function. In particular, during the first 3 days of EC attachment on 2D hydrogels, the fast-relaxing hydrogels generally supported greater cell spreading than slow-relaxing hydrogels at the same stiffness. Within 3D hydrogels, the fast-relaxing hydrogels at low- and medium-stiffness, as well as the slow-relaxing hydrogels with low stiffness supported vascular sprouting. In particular, the branches were significantly wider in the low-stiffness hydrogels, compared with the medium- and high-stiffness hydrogels. When implanted in vivo, the fast-relaxing, low-stiffness hydrogel promoted significantly more vascularization compared with the slow-relaxing hydrogels. Overall, these findings suggest that the fast-relaxing, low-stiffness ELP-PEG hydrogel may be a suitable choice for supporting 3D vascularization in vivo.

Our work revealed an important role of stress relaxation rate in the modulation of endothelial behavior. ECs naturally reside in blood vessels that experience some degree of stress relaxation, while still maintaining physiological blood pressure. During the process of vascularization, ECs degrade and remodel the ECM, in parallel with sprouting and branching.[41–43] The potential signaling mechanism by which stress relaxation rate modulates endothelial behavior may be related to integrin clustering, which is necessary for focal adhesion formation, migration, and vascular formation.[37] This is supported by a recent report showing notable differences in microvessel formation between stress-relaxing and nonstress-relaxing gels.[44] In particular, the authors demonstrated that stress-relaxing hydrogels promoted integrin clustering and focal adhesion kinase activation, with greater motility for angiogenesis compared with nonstress-relaxing hydrogels. In other cell types, stress relaxation rate significantly alters cell morphology and gene activation.[14,15,45] Consistent with our findings of fast-relaxing hydrogels being beneficial, Chaudhuri et al.[15] showed that fast-relaxing hydrogels enhanced mesenchymal cell spreading, proliferation, and osteogenic differentiation . Mechanistically, the effects of stress relaxation rate were associated with adhesion-ligand binding, actomyosin contractility, and mechanical clustering of cell-adhesion ligands. Previous studies have also found that matrix stiffness and stress relaxation rates can impact cell secretion of pro-angiogenic growth factors and cytokines.[13,46,47] Our findings support a growing literature that fast-relaxing hydrogels may be beneficial for EC culture. These results suggest that stress relaxation rate is an important design criterion for tissue engineering.

While the ELP-PEG hydrogel system allows for decoupling of matrix stiffness and stress relaxation rate, we note that additional matrix properties remain linked. As a result, formulation changes to increase stiffness or stress relaxation rate can also alter other aspects of the hydrogel, such as ligand presentation and degradation rate. For example, matrix stiffness is modulated by changing the concentration of ELP, which thereby changes the concentration of RGD peptide presented to the cells. Prior literature suggests that increased vascular sprouting in 3D is correlated with higher RGD concentrations.[48] Interestingly, we observe that our low-stiffness hydrogels with lower RGD concentration promoted vascular sprouting in 3D. These results suggest a potential interaction between matrix stiffness and adhesive

ligand density for the stiffness range presented here. In addition, altering the on–off rate of crosslinks by swapping the PEG-ALD and PEG-BZA may lead to differences in degradation rate, with faster on–off rates resulting in faster degradation. As we continue to explore the dynamic and complex field of cell–ECM interactions, we must consider the intricate interplay of these matrix properties and how they work both together and separately to influence endothelial behavior. Therefore, it is beneficial to explore new and alternative strategies, such as the dynamic hydrogels presented here, for independent tuning of specific hydrogel properties.

Dynamic hydrogels formed by ELP-HYD with PEG-BZA or PEG-ALD have the capacity to shear-thin and rapidly regain their mechanical properties after being extruded from a syringe. The resulting hydrazone bond can quickly reform and regain its stiffness within seconds. This makes hydrogel formation based on these bonds attractive for in vivo applications that require the deposition of materials in an irregular cavity or active tissues, as they prevent the hydrogel from being dispersed. However, there are some reported drawbacks in using bonds that can quickly reform, particularly concerning degradation of the materials. These effects are amplified in fast stress-relaxing hydrogels in in vitro culture, where the hydrogels are exposed to a large volume of liquid cell culture medium. The polymers that make up these materials can be easily solvated and washed away. To demonstrate that our hydrogels can be fast stress-relaxing and be retained for an extended amount of time in vivo, our experimental conditions were implanted subcutaneously in mice. Interestingly, we found that the low-stiffness conditions had a higher retention percentage than the high-stiffness experimental conditions. This result suggests that the stress-relaxation rate did not play a substantial role in the in vivo biodegradation rate of ELP-PEG materials. In these conditions, it is possible that the higher retention was due to the stoichiometry imbalance between ALD/BZA motifs to HYD motifs in the low-stiffness gels (2.67:1 ALD:HYD; 3.75:1 BZA:HYD) compared with the high-stiffness gels (4.28:1 ALD:HYD; 5.35:1 BZA:HYD). Alternatively, the encapsulated cells may alter their secretion of proteases in the different ELP-PEG hydrogels, which might alter the rate of enzymatic biodegradation. We demonstrated that several hydrogel formulations, including the fast-relaxing, low-stiffness hydrogel that produced the best vascularization outcome, could be retained for at least 14 days.

The ELP hydrogels are well-suited for in vivo implantation, owing to their injectability, shear thinning capacity, biodegradability, and safety. Despite the small sample size of the subcutaneous implantation study, we show that the mice tolerated the hydrogel implantations without adverse effects, and the hydrogel formulations showed varying degrees of degradation. However, larger sample sizes may be necessary to confirm the in vivo findings. In addition, implanting cell-seeded ELP-PEG hydrogels into disease tissues such as ischemic muscle may further validate the potential of the cell-seeded scaffolds to promote angiogenesis in a more therapeutically relevant setting.

Finally, we acknowledge some limitations in the design of the in vitro studies. Since the 2D and 3D experiments varied in cellular composition and seeding density, it is not feasible to make direct, quantitative comparisons of cellular responses between the 2D and 3D environments. In addition, since the experiments in 3D consisted of cocultured cells, the relative contribution of the ECs to gene expression levels could not be distinguished from that of the fibroblasts. Despite these limitations, we believe this family of ELP-PEG hydrogels enables the study of endothelial behavior in well-defined mechanical environments.

5 | CONCLUSION

In conclusion, we engineered a family of ELP-PEG hydrogels that harness DCC crosslinking for shear-thinning properties, while also having controllable stiffness and stress relaxation rate. Using a range of stiffness and stress relaxation rates, we showed that fast-relaxing 2D hydrogels promoted greater cell spreading area at early time points compared with slow-relaxing hydrogels of the same stiffness. In 3D cell-encapsulating hydrogels, the fast-relaxing, medium-stiffness hydrogels supported longer branches, whereas the fast-relaxing, low-stiffness formulation induced wider vascular branches compared with those from slow-relaxing hydrogels. In a subcutaneous implantation model, the fast-relaxing, low-stiffness hydrogel promoted higher capillary density compared with the slow-relaxing, low-stiffness hydrogel. These studies suggest that stress relaxation rate is an important mechanical modulator of endothelial function. The findings from this study have important implications in the design of biomaterials to support vascularization within engineered tissues.

AUTHOR CONTRIBUTIONS

Mahdis Shayan, Ngan F. Huang, and Sarah C. Heilshorn designed the experiments. Mahdis Shayan, Michelle S. Huang, Renato Navarro, Gladys Chiang, Caroline Hu, Patrik K. Johansson, Abbygail A. Foster, Bauer L. LeSavage, Julien G. Roth, Riley A. Suhar, and Maedeh Zamani performed the experiments. Mahdis Shayan, Beu P. Oropeza, Gladys Chiang, and Ngan F. Huang analyzed the data. Mahdis Shayan, Ngan F. Huang, and Sarah C. Heilshorn interpreted the data. Mahdis Shayan, Michelle S. Huang, Renato Navarro, and Ngan F. Huang wrote the manuscript, with input from all authors. All authors have read and approved the final manuscript.

ACKNOWLEDGMENTS

This work was supported in part by grants from the US National Institutes of Health (R01 HL127113 and R01 HL142718 to Ngan F. Huang; R21 NS114549, R01 EB027666, R01 EB027171, R01 HL151997 to Sarah C. Heilshorn), the US Department of Veterans Affairs (1I01BX002310, 1I01BX004259, RX001222 to Ngan F. Huang), the National Science Foundation (1829534 to Ngan F. Huang and CBET 2033302 and DMR 2103812 to Sarah C. Heilshorn), and the American Heart Association (20IPA35360085 and 20IPA35310731 to Ngan F. Huang; 903771 to Renato Navarro).

CONFLICT OF INTEREST STATEMENT

The authors report no competing interests.

DATA AVAILABILITY STATEMENT

All data generated are available upon reasonable request.

ORCID

Ngan F. Huang https://orcid.org/0000-0003-2298-6790

REFERENCES

1. Gimbrone MA Jr, Topper JN, Nagel T, Anderson KR, Garcia-Cardena G. Endothelial dysfunction, hemodynamic forces, and atherogenesis. *Ann N Y Acad Sci*. 2000;902:230-239.
2. Davignon J, Ganz P. Role of endothelial dysfunction in atherosclerosis. *Circulation*. 2004;109:III27-III32.
3. Huebsch N, Arany PR, Mao AS, et al. Harnessing traction-mediated manipulation of the cell/matrix interface to control stem-cell fate. *Nat Mater*. 2010;9:518-526.
4. Lo CM, Wang HB, Dembo M, Wang YL. Cell movement is guided by the rigidity of the substrate. *Biophys J*. 2000;79:144-152.
5. Engler AJ, Sen S, Sweeney HL, Discher DE. Matrix elasticity directs stem cell lineage specification. *Cell*. 2006;126:677-689.
6. Zamani M, Cheng YH, Charbonier F, et al. Single-cell transcriptomic census of endothelial changes induced by matrix stiffness and the association with atherosclerosis. *Adv Funct Mater*. 2022;32:2203069. doi:10.1002/adfm.202203069
7. Huang NF, Patlolla B, Abilez O, et al. A matrix micropatterning platform for cell localization and stem cell fate determination. *Acta Biomater*. 2010;6:4614-4621.
8. Huang NF, Chu J, Lee RJ, Li S. Biophysical and chemical effects of fibrin on mesenchymal stromal cell gene expression. *Acta Biomater*. 2010;6:3947-3956.
9. Hou L, Coller J, Natu V, Hastie TJ, Huang NF. Combinatorial extracellular matrix microenvironments promote survival and phenotype of human induced pluripotent stem cell-derived endothelial cells in hypoxia. *Acta Biomater*. 2016;44:188-199.
10. Hou L, Kim JJ, Wanjare M, et al. Combinatorial extracellular matrix microenvironments for probing endothelial differentiation of human pluripotent stem cells. *Sci Rep*. 2017;7:6551.
11. Madl CM, LeSavage BL, Dewi RE, et al. Maintenance of neural progenitor cell stemness in 3d hydrogels requires matrix remodelling. *Nat Mater*. 2017;16:1233-1242.
12. Benitez PL, Mascharak S, Proctor AC, Heilshorn SC. Use of protein-engineered fabrics to identify design rules for integrin ligand clustering in biomaterials. *Integr Biol (Camb)*. 2016;8:50-61.
13. Cai L, Dewi RE, Goldstone AB, et al. Regulating stem cell secretome using injectable hydrogels with in situ network formation. *Adv Healthc Mater*. 2016;5:2758-2764.
14. Chaudhuri O, Gu L, Darnell M, et al. Substrate stress relaxation regulates cell spreading. *Nat Commun*. 2015;6:6364.
15. Chaudhuri O, Gu L, Klumpers D, et al. Hydrogels with tunable stress relaxation regulate stem cell fate and activity. *Nat Mater*. 2016;15:326-334.
16. Sommerfeld SD, Elisseeff JH. Time to relax: mechanical stress release guides stem cell responses. *Cell Stem Cell*. 2016;18:166-167.
17. Betre H, Setton LA, Meyer DE, Chilkoti A. Characterization of a genetically engineered elastin-like polypeptide for cartilaginous tissue repair. *Biomacromolecules*. 2002;3:910-916.
18. Wang H, Zhu D, Paul A, et al. Covalently adaptable elastin-like protein - hyaluronic acid (elp - ha) hybrid hydrogels with secondary thermoresponsive crosslinking for injectable stem cell delivery. *Adv Funct Mater*. 2017;27:1605609.
19. Hunt DR, Klett KC, Mascharak S, et al. Engineered matrices enable the culture of human patient-derived intestinal organoids. *Adv Sci (Weinh)*. 2021;8:2004705.
20. Chaudhuri O, Cooper-White J, Janmey PA, Mooney DJ, Shenoy VB. Effects of extracellular matrix viscoelasticity on cellular behaviour. *Nature*. 2020;584:535-546.
21. LeSavage BL, Suhar NA, Madl CM, Heilshorn SC. Production of elastin-like protein hydrogels for encapsulation and immunostaining of cells in 3d. *JoVE*. 2018;135:e57739.
22. Navarro RS, Huang MS, Roth JG, et al. Tuning polymer hydrophilicity to regulate gel mechanics and encapsulated cell morphology. *Adv Healthc Mater*. 2022;11:2200011.
23. Wang H, Paul A, Nguyen D, Enejder A, Heilshorn SC. Tunable control of hydrogel microstructure by kinetic competition between self-assembly and crosslinking of elastin-like proteins. *ACS Appl Mater Interfaces*. 2018;10:21808-21815.
24. Suhar RA, Marquardt LM, Song S, et al. Elastin-like proteins to support peripheral nerve regeneration in guidance conduits. *ACS Biomater Sci Eng*. 2021;7:4209-4220.
25. Krafft C, Dietzek B, Schmitt M, Popp J. Raman and coherent anti-stokes raman scattering microspectroscopy for biomedical applications. *J Biomed Opt*. 2012;17:040801.
26. Lau S, Gossen M, Lendlein A, Jung F. Venous and arterial endothelial cells from human umbilical cords: potential cell sources for cardiovascular research. *Int J Mol Sci*. 2021;22:978.
27. Zaitseva TS, Alcazar C, Zamani M, et al. Aligned nanofibrillar scaffolds for controlled delivery of modified mrna. *Tissue Eng Part A*. 2019;25:121-130.
28. Nakayama KH, Alcazar C, Yang G, et al. Rehabilitative exercise and spatially patterned nanofibrillar scaffolds enhance vascularization and innervation following volumetric muscle loss. *NPJ Regen Med*. 2018;3:16.
29. Huang NF, Yu J, Sievers R, Li S, Lee RJ. Injectable biopolymers enhance angiogenesis after myocardial infarction. *Tissue Eng*. 2005;11:1860-1866.
30. Hou L, Yang G, Tang S, et al. Small molecule derived from carboxyethylpyrrole protein adducts promotes angiogenesis in a mouse model of peripheral arterial disease. *J Am Heart Assoc*. 2018;7:e009234.
31. Madl CM, Heilshorn SC. Tyrosine-selective functionalization for bio-orthogonal cross-linking of engineered protein hydrogels. *Bioconjug Chem*. 2017;28:724-730.
32. Huang NF, Fleissner F, Sun J, Cooke JP. Role of nitric oxide signaling in endothelial differentiation of embryonic stem cells. *Stem Cells Dev*. 2010;19:1617-1626.
33. Straley KS, Heilshorn SC. Independent tuning of multiple biomaterial properties using protein engineering. *Soft Matter*. 2009;5:114-124.
34. Vargas-Pinto R, Gong H, Vahabikashi A, Johnson M. The effect of the endothelial cell cortex on atomic force microscopy measurements. *Biophys J*. 2013;105:300-309.
35. Wood JA, Liliensiek SJ, Russell P, Nealey PF, Murphy CJ. Biophysical cueing and vascular endothelial cell behavior. *Materials*. 2010;3:1620-1639.
36. Lee SY, Zaske AM, Novellino T, et al. Probing the mechanical properties of tnf-alpha stimulated endothelial cell with atomic force microscopy. *Int J Nanomedicine*. 2011;6:179-195.
37. Charbonier FW, Zamani M, Huang NF. Endothelial cell mechanotransduction in the dynamic vascular environment. *Adv Biosyst*. 2019;3:e1800252.
38. Lou J, Stowers R, Nam S, Xia Y, Chaudhuri O. Stress relaxing hyaluronic acid-collagen hydrogels promote cell spreading, fiber remodeling, and focal adhesion formation in 3d cell culture. *Biomaterials*. 2018;154:213-222.
39. Costa-Almeida R, Gomez-Lazaro M, Ramalho C, Granja PL, Soares R, Guerreiro SG. Fibroblast-endothelial partners for vascularization strategies in tissue engineering. *Tissue Eng Part A*. 2015;21:1055-1065.

40. Newman AC, Nakatsu MN, Chou W, Gershon PD, Hughes CC. The requirement for fibroblasts in angiogenesis: fibroblast-derived matrix proteins are essential for endothelial cell lumen formation. *Mol Biol Cell*. 2011;22:3791-3800.
41. Crosby CO, Zoldan J. Mimicking the physical cues of the ecm in angiogenic biomaterials. *Regen Biomater*. 2019;6:61-73.
42. Davis GE, Bayless KJ. An integrin and rho gtpase-dependent pinocytic vacuole mechanism controls capillary lumen formation in collagen and fibrin matrices. *Microcirculation*. 2003;10:27-44.
43. Davis GE, Senger DR. Endothelial extracellular matrix: biosynthesis, remodeling, and functions during vascular morphogenesis and neovessel stabilization. *Circ Res*. 2005;97:1093-1107.
44. Wei Z, Schnellmann R, Pruitt HC, Gerecht S. Hydrogel network dynamics regulate vascular morphogenesis. *Cell Stem Cell*. 2020;27:798-812.
45. McKinnon DD, Domaille DW, Cha JN, Anseth KS. Biophysically defined and cytocompatible covalently adaptable networks as viscoelastic 3d cell culture systems. *Adv Mater*. 2014;26:865-872.
46. Phuagkhaopong S, Mendes L, Muller K, et al. Silk hydrogel substrate stress relaxation primes mesenchymal stem cell behavior in 2d. *ACS Appl Mater Interfaces*. 2021;13:30420-30433.
47. Foster AA, Dewi RE, Cai L, et al. Protein-engineered hydrogels enhance the survival of induced pluripotent stem cell-derived endothelial cells for treatment of peripheral arterial disease. *Biomater Sci*. 2018;6:614-622.
48. Nguyen EH, Zanotelli MR, Schwartz MP, Murphy WL. Differential effects of cell adhesion, modulus and vegfr-2 inhibition on capillary network formation in synthetic hydrogel arrays. *Biomaterials*. 2014;35:2149-2161.

SUPPORTING INFORMATION

Additional supporting information can be found online in the Supporting Information section at the end of this article.

How to cite this article: Shayan M, Huang MS, Navarro R, et al. Elastin-like protein hydrogels with controllable stress relaxation rate and stiffness modulate endothelial cell function. *J Biomed Mater Res*. 2023;1-14. doi:10.1002/jbm.a.37520